# Near-resonance scattering of the para-$H_2$ vibrons in (ortho-$H_2$)$_x$(para-$H_2$)$_{1-x}$ mixed crystals

J. De Kinder, A. Bouwen, and D. Schoemaker
*Physics Department, University of Antwerp (U.I.A.), B-2610 Antwerp (Wilrijk), Belgium*

A. Boukahil and D.L. Huber*
*Synchrotron Radiation Center, University of Wisconsin–Madison, Stoughton, Wisconsin 53589*
(Received 17 September 1993)

The $p$-$H_2$ vibrons have been studied by high-resolution Raman scattering in mixed crystals of ($o$-$H_2$)$_x$($p$-$H_2$)$_{1-x}$, (HD)$_x$($p$-$H_2$)$_{1-x}$, and ($o$-$D_2$)$_{0.069}$($p$-$H_2$)$_{0.931}$. For increasing $o$-$H_2$ concentration, the line shape broadens and becomes asymmetric with a tail towards higher frequencies. This effect is less pronounced in the HD- and the $o$-$D_2$-doped crystals, where the energy difference between the $p$-$H_2$ vibron and the stretching vibration of the impurity is much larger. Isolated impurities still have a symmetrical line shape, showing that the asymmetry is not due to inhomogeneities. Calculated line shapes by the coherent-potential-approximation technique are in very good qualitative agreement with the experimental results. The theory also accounts for previously published experimental data on the variations of the relative positions and intensities of the ortho and para peaks in ($o$-$H_2$)$_x$($p$-$H_2$)$_{1-x}$.

## I. INTRODUCTION

The interaction between vibrational excitations accounts for the nonvanishing linewidth of these states. These processes are temperature dependent through the population numbers of the states involved in these processes. The linewidths of both acoustical and optical phonons in molecular crystals have been extensively studied and are now well understood.[1] In general, the line broadening contributions or the corresponding dephasing times (given by the $T_2$ time) can be divided into decay towards other vibrational states ($T_1$ time) and into pure dephasing processes of the generated excitations. By increasing the number of vibrational states in the crystal, more pathways become available and the line broadening will increase.

In the case of substitutional disorder, inhomogeneous contributions to the linewidth may occur due to the mismatch in size between the impurity and the lattice parameter of the host matrix. This may mask an increase in the homogeneous relaxation rate, as was observed in, e.g., naphtalene-$d_8$/naphtalene-$h_8$ (Ref. 2), $\alpha$-(Ar)$_x$($N_2$)$_{1-x}$ (Ref. 3), and in $\alpha$-($^{14}N_2$)$_{1-x}$($^{15}N_2$)$_x$ mixed crystals.[4] In ($o$-$H_2$)$_x$($p$-$H_2$)$_{1-x}$ mixed crystals, both constituents are formed by different rotational states ($J = 0, 2, 4, \ldots$ for $p$-$H_2$ and $J = 1, 3, 5, \ldots$ for $o$-$H_2$) of the same molecule. Thereby it forms an ideal mixed molecular crystal to study the effect of disorder in.

In this paper, we will concentrate on the first vibrational transition $Q_1(0)$ of the $p$-$H_2$ molecule ($\Omega_v$=4149.7 cm$^{-1}$, Ref. 5). In the pure $p$-$H_2$ crystal, the vibrational states on individual molecules couple and form wavelike states. This crystal states are analogous to Frenkel excitons. The $Q_1(1)$ vibrational transition of $o$-$H_2$ in the pure $o$-$H_2$ crystal is $2\Delta(o\text{-}H_2)$ = 6-7 cm$^{-1}$ lower than the $p$-$H_2$ frequency. The bandwidth $W$ of the $p$-$H_2$ vibrons was estimated to be 4 cm$^{-1}$ (Ref. 6), so that we are just within the separated bands limit $2\Delta(o\text{-}H_2) > W$. These stretching vibrations are well separated from other excitations in the medium, as low-frequency phonons (0–80 cm$^{-1}$) and rotational excitations (ranging from 179 cm$^{-1}$ for $o$-$D_2$ up to 587 cm$^{-1}$ for $o$-$H_2$). This explains the very long $T_1$ time of 7.5 $\mu$s for normal $H_2$.[7]

The vibrational transitions under study have already been investigated by low-resolution ($\sim$ 0.1 cm$^{-1}$) spontaneous Raman scattering[5] and by time-resolved coherent anti-Stokes Raman scattering.[8] While the first suffer from a too low resolution of their setup, only a small concentration region ($0.0022 < x < 0.027$) was studied in the latter. We have performed high-resolution measurements of spontaneous Raman scattering off the $p$-$H_2$ vibron states in mixed crystals of ($o$-$H_2$)$_x$($p$-$H_2$)$_{1-x}$ for $0.006 < x < 0.626$. In Ref. 8, plausible arguments were given for the occurrence of near-resonance scattering, although clear evidence for this can be found by comparing the results to HD or $D_2$ doped crystals.[9] In these mixed crystals, the impurities have a vibrational frequency which is much more separated from the $p$-$H_2$ transition, i.e., for HD: $\Omega_v$ = 3633 cm$^{-1}$ and for $D_2$: $\Omega_v$ = 2994 cm$^{-1}$.

The main interaction among the molecules in ($o$-$H_2$)$_x$($p$-$H_2$)$_{1-x}$ mixed crystals is the van der Waals interaction which is essentially independent of the rotational state of the molecule. This makes that the interactions among host molecules and between host molecules and impurities are comparable. Hence the coherent poten-

 

tial approximation (CPA),[10] which is well established for Frenkel excitons in substitutionally disordered molecular crystals,[11] can be applied for the calculation of the line shape of the $\mathbf{k} \simeq \mathbf{0}$ vibrational states in the mixed crystals. In this paper we will show that the CPA is well suited to this calculation. Other experimental quantities are also predicted by the CPA scheme. These include the relative position[5] of the $Q_0(1)$ and the $Q_1(1)$ line and the intensity[12,13] ratio of the $Q_1(1)$ transition relative to $Q_0(1)$, which is "anomalously" larger than one would expect from the concentration ratio. As far as we know, this is the first application of the CPA technique to describe delocalized vibrational states in molecular crystals, although in the past it has been applied to the characterization of the vibrational line shapes of interacting molecules adsorbed on surfaces.[14]

Experimental line shapes of the $p$-$H_2$ vibron states in mixed crystals of $(o\text{-}H_2)_x(p\text{-}H_2)_{1-x}$, $(HD)_x(p\text{-}H_2)_{1-x}$, and $(o\text{-}D_2)_{0.069}(p\text{-}H_2)_{0.931}$ are presented in Sec. III. This section also contains the line shape of the $o$-$D_2$ localized vibrational state in $(o\text{-}D_2)_{0.025}(p\text{-}H_2)_{0.907}(o\text{-}H_2)_{0.068}$. Section IV describes the model used to calculate the spectra and the results obtained with it. Further discussion and conclusions are drawn in Sec. V.

## II. EXPERIMENTAL

Research grade gases (99.9999% for $H_2$, 98% for HD, and 99.8% for $D_2$) were used as the starting material. The main impurities for HD are $H_2$, while for $D_2$ also $N_2$ is present. The latter is trapped during the catalysis process, resulting in a higher purity than stated. The catalysis of normal hydrogen gas to nearly pure para-$H_2$ and the growth of single-crystals is described in Ref. 15. Small amounts of HD gas and $D_2$ gas were admixed in the gas phase before the catalysis.

The concentration of $o$-$D_2$, HD, $p$-$H_2$, and $o$-$H_2$ species was determined from the integrated intensity of their respective lowest $\Delta J = 2$ transition in the liquid phase, as determined by spontaneous Raman scattering.[16] No trace of $p$-$D_2$ impurities were found due to the much lower ortho-para conversion rate for $D_2$ as compared to $H_2$.[17] No change in the $o$-$H_2$ concentration was found before growing the crystal and after performing the measurements. Neither was any difference found between the liquid and the solid phase.

Scattered light from a single-frequency $Ar^+$ laser (454.5 nm) was collected in a backscattering geometry. After spatially filtering it was sent through the combination of a single pass piezoelectrically scanned Fabry-Perot interferometer (finesse $F \approx 38$) and a monochromator. The monochromator served as a broad passband filter and was centered at the vibrational transition under study. The resolution of the setup can be varied by changing the distance between the mirrors of the Fabry-Perot. Due to the large Stokes shift (4150 $cm^{-1}$) of the scattered light and the variation of the reflectivity $R(\lambda)$ of the mirrors with wavelength, the elastically scattered light can no longer be used to obtain the resolution function of the setup. An Airy function was calculated starting from a measured value for $R(\lambda$=560.5 nm) and was used as a resolution function to deconvolute the spectra, so that linewidths down to 0.002 $cm^{-1}$ can be measured. This high resolution can only be obtained with excitation at 454.5 nm which, due to the lower gain of this laser line, limited the available power of the $Ar^+$ laser to 35 mW.

All measurements were performed at 6 K. No temperature dependence of the line shape was found in any crystal.

## III. EXPERIMENTAL RESULTS

### A. $(o\text{-}H_2)_x(p\text{-}H_2)_{1-x}$ mixed crystals

In Figs. 1 and 2, the $p$-$H_2$ line shape for several concentrations of $o$-$H_2$ molecules is shown. For $x = 0.006$, the linewidth is within the experimental resolution. For $x = 0.013$, the line broadens and is asymmetric with a tail towards higher frequencies. For increasing $o$-$H_2$ concentrations, the width of the line increases and the asymmetry becomes more pronounced. For $o$-$H_2$ concentrations above 30 %, i.e., well within the mixed crystal regime, the line shapes of both the $o$-$H_2$ and the $p$-$H_2$ transition are more complicated.

Our measurements indicate that the processes contributing to the linewidth occur on a ps or ns timescale. This shows that the population relaxation of the $p$-$H_2$ vibron, which was determined to be $T_1 = 7.5$ $\mu$s,[7] has only a negligible contribution to the linewidth. The line broadening process can be fully ascribed to pure dephasing processes.

Abram *et al.*[8] performed ns time-domain dephasing measurements on the $p$-$H_2$ states. They found essentially a decay which is slower than exponential (stretched exponential), with an effective decay constant that increases with increasing $o$-$H_2$ concentration. Our frequency-domain measurements provide more information than the time-domain results, which is contained in the asymme-

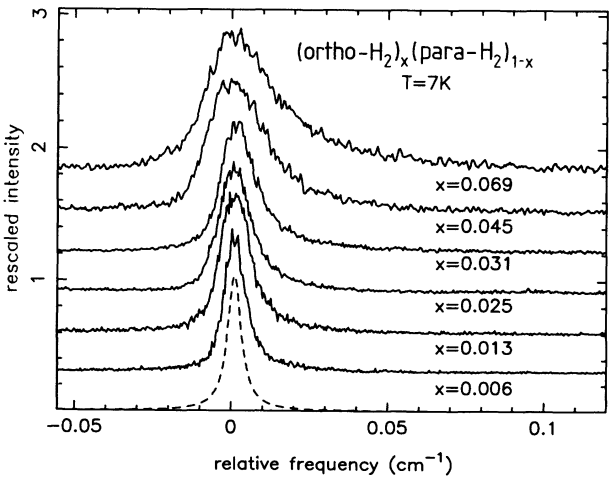


FIG. 1. High-resolution spectrum of the $p$-$H_2$ vibron in mixed crystals of $(o\text{-}H_2)_x(p\text{-}H_2)_{1-x}$ for a varying $x$. The broken line indicates the resolution function of the setup.

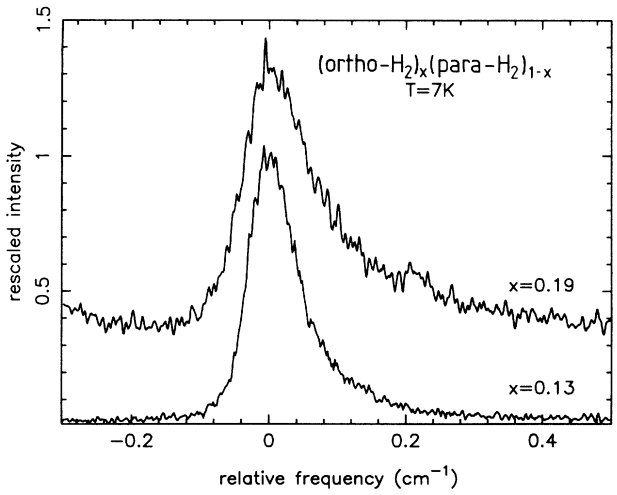


FIG. 2. High-resolution spectrum of the $p$-$H_2$ vibron in mixed crystals of $(o\text{-}H_2)_x(p\text{-}H_2)_{1-x}$ for a varying $x$.

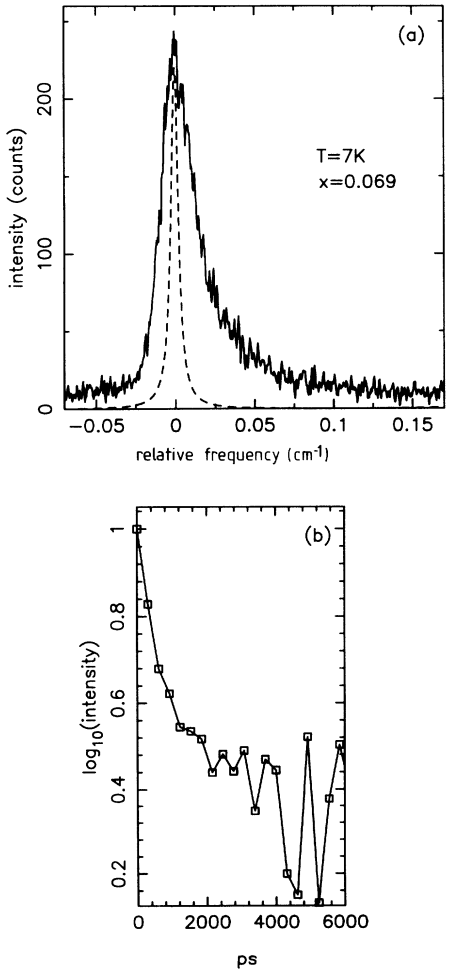


FIG. 3. High-resolution spectrum [(a), full line] of the $p$-$H_2$ vibron in a mixed crystal with 6.9% $o$-$H_2$ impurities. The resolution of the setup is indicated by the broken line. (b) shows the corresponding Fourier transform of the Raman spectrum. The dephasing is clearly faster than exponential.

try of the line shape.[3] In order to compare our measurements with theirs, we Fourier transformed our results. In Fig. 3(a) the linewidth of the $p$-$H_2$ vibron for $x$=0.069 % is shown together with its Fourier transform [Fig. 3(b)]. The obtained dephasing signal decays also faster than exponential, in accordance with the results of Ref. 8. We also find an increasing effective decay rate with increasing $o$-$H_2$ concentration and the same behavior for higher $o$-$H_2$ concentrations on the ps time scale. This identical behavior on different time scales is in contrast to dephasing signals for the vibrons in $\alpha$-$N_2$,[4,18] where we found a faster-than-exponential dephasing on the ps time scale, while on the ns time scale, a slower-than-exponential decay was found.

For $x = 0.013$, we obtain a linewidth which is slightly larger than the experimental resolution of 0.002 $cm^{-1}$. This indicates that the observed linewidth of 0.0014 $cm^{-1}$ in a mixed crystal with 0.06 % $o$-$H_2$ by Momose *et al.*[19] is most probably due to the insufficient resolution of their setup.

### B. $(HD)_x(p\text{-}H_2)_{1-x}$ and $(o\text{-}D_2)_{0.069}(p\text{-}H_2)_{0.931}$ mixed crystals

A test for the occurrence of near-resonant scattering is to compare the effect of doping with $o$-$H_2$ to doping with HD or $o$-$D_2$ molecules. These have a much larger frequency difference to the $p$-$H_2$ vibron states, so that the scattering off these impurities is much more off resonance. In Fig. 4, the line shapes of the $p$-$H_2$ vibron are shown for three concentrations of HD. For the lowest concentration of HD, $x$= 0.084, no asymmetry can be observed in the line shape. A Gaussian with a full width at half maximum (FWHM) = 0.004 ± 0.001 $cm^{-1}$ could be well fitted to it. This indicates the presence of still some inhomogeneous line broadening effects for isotopic substitution. For 11.7 % HD doping, the spectrum is already clearly asymmetric with a tail towards high frequencies. The global width and the asymmetry of the transition

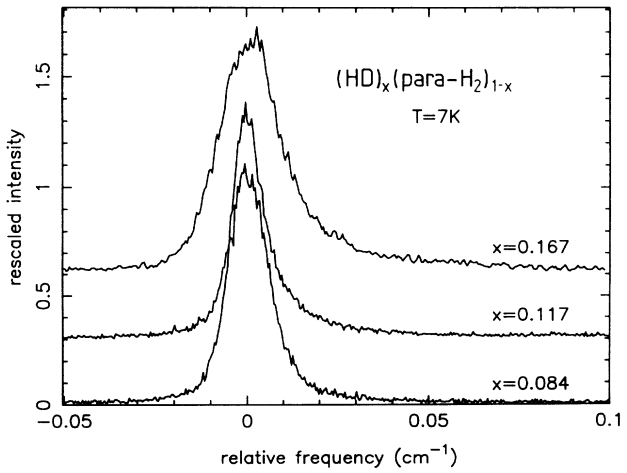


FIG. 4. High-resolution spectrum of the line shape of the $p$-$H_2$ vibron in a mixed crystal of $(HD)_x(p\text{-}H_2)_{1-x}$ for various HD concentrations.

become larger for the highest HD concentration which was studied (16.7 %).

The linewidth of the $p$-$H_2$ vibron in the $(o\text{-}D_2)_{0.069}(p\text{-}H_2)_{0.931}$ mixed crystal is close to the resolution of the setup, which is in agreement with the results obtained for HD. Therefore no crystals with a larger $o$-$D_2$ content were investigated.

From the comparison of Figs. 1 and 2 with Fig. 4, we see that doping with $o$-$H_2$ molecules has a more profound effect on the line shape. The global width and the asymmetry are more pronounced in the $(o\text{-}H_2)_x(p\text{-}H_2)_{1-x}$ mixed crystals than in the $(HD)_x(p\text{-}H_2)_{1-x}$ and the $(o\text{-}D_2)_{0.069}(p\text{-}H_2)_{0.931}$ mixed crystals for an equal concentration of dopants.

### C. $(o\text{-}D_2)_{0.025}(p\text{-}H_2)_{0.907}(o\text{-}H_2)_{0.068}$ mixed crystal

In order to eliminate inhomogeneous line broadening as a possible cause for the asymmetric line shape of the delocalized $p$-$H_2$ vibrons, we investigated the effect of a substantial $o$-$H_2$ doping on the line shape of localized vibrational states. The relatively high concentration of the $o$-$H_2$ together with the electrostatic quadrupole-quadrupole interaction among the $J = 1$ species, makes that the $Q_1(1)$ transition of $H_2$ is not an ideal probe. Therefore, we included a concentration of 2.5 % $o$-$D_2$ into the crystal. This small concentration is known to have but a negligible influence on the $p$-$H_2$ line shape (see Sec. III B). As can be seen from Fig. 5, the vibrational transition of the $o$-$D_2$ dopants has a symmetrical line shape and is relatively well described by a Lorentzian with FWHM $= 0.025 \pm 0.007$ cm$^{-1}$. This shows that the asymmetry of the $p$-$H_2$ line shape is not due to inhomogeneous line broadening caused by different local environments.

The width of the $o$-$D_2$ transition increases with increasing $o$-$H_2$ concentration, since for an $o$-$H_2$ concentration of 0.06 %, a linewidth of 0.004 cm$^{-1}$ was found.[20]

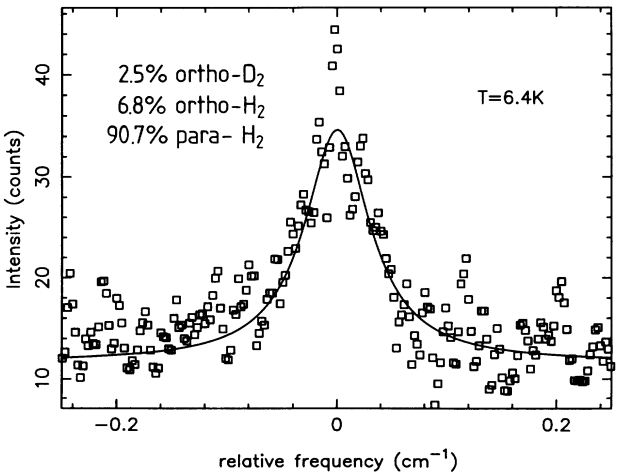


FIG. 5. High-resolution spectrum of the line shape of isolated $o$-$D_2$ impurities in a mixed crystal with 6.8 % $o$-$H_2$ molecules. The solid line is the best fitting Lorentzian to the experimental data points (denoted by □).

## IV. MODEL

In this section, we present the results of a theoretical study of the effects of $o$-$H_2$ and HD doping on the $p$-$H_2$ vibron line shape. Our approach is based on the coherent potential approximation (CPA) for the optical line shape function. Since the details of the CPA for optical line shapes have been presented elsewhere,[11,21] we will consider only its application to the problem at hand.

In the CPA, the optical line shape function is given by an expression of the form

$$f(E) = \frac{1}{\pi}\mathrm{Im}\left[\frac{1}{E - V_c(E)}\right], \tag{4.1}$$

where Im denotes the imaginary part. The "coherent potential," $V_c(E)$, is the solution of the equation

$$\int dV P(V)\frac{V - V_c(E)}{1 - [V - V_c(E)]G_o[E - V_c(E)]} = 0, \tag{4.2}$$

in which $P(V)$ is the distribution of intramolecular vibration frequencies, and the Green's function, $G_o(E)$, is expressed in terms of the energies of the vibron modes.

In applying the CPA formalism to $H_2$, we make two additional approximations. First, we substitute a fcc lattice with nearest-neighbor interactions for the hcp lattice of solid $H_2$.[13] Second, we assume that the ortho-para, the ortho-ortho, the HD-HD, and the HD-para interactions are all equal to the coupling between para molecules. Under these conditions, $G_o$ is given by the expression

$$G_o(E) = \frac{1}{N}\sum_{\mathbf{k}}\frac{1}{\{E - [E(\mathbf{k}) - E(0)]\}}, \tag{4.3}$$

where the sum is over the $N$ wave vectors spanning the Brillouin zone of the fcc lattice, and the symbol $E(\mathbf{k})$ denotes the energy of a vibron with wave vector $\mathbf{k}$.

The distribution of intramolecular vibrational frequencies is taken to be of the form

$$P(V) = x\delta(V + \Delta) + (1 - x)\delta(V - \Delta), \tag{4.4}$$

where $x$ is the concentration of $o$-$H_2$ or HD molecules and $(1 - x)$ denotes the $p$-$H_2$ concentration. The parameter $\Delta$ is identified as one-half the difference between the intramolecular transition frequencies of $p$-$H_2$ and $o$-$H_2$ or HD. In the ortho-para analysis, $\Delta$ is set equal to 3 cm$^{-1}$ (which is the value appropriate to the gas phase[13]), whereas in the HD-para calculation, we take $\Delta$ equal to 264.5 cm$^{-1}$.[17,22]

After inserting Eq. (4.4) into Eq. (4.2) and evaluating the integral over V, we obtain the equation

$$V_c - (1 - 2x)\Delta - (\Delta^2 - V_c^2)G_o(E - V_c) = 0. \tag{4.5}$$

In order to carry out detailed calculations, one needs either a numerical or analytic expression of the Green's function for complex energies. Since our interest is in the behavior near the peaks in the spectrum for relatively low impurity concentrations, we have used a low-energy approximation to $G_o(E)$ obtained by keeping the

two lowest-order terms in the expansion about $E = 0$, i.e.,[21,23]

$$G_o(E) = \frac{-1.792}{W} + \frac{1.273\sqrt{-E}}{W^{3/2}} \tag{4.6}$$

for the fcc lattice with nearest-neighbor interactions. Here $W$ denotes the width of the vibron band in pure $p$-$H_2$, which we take equal to 4 $cm^{-1}$ (Ref. 13).

Equations (4.1), (4.5), and (4.6) allow one to calculate the Raman line shape for arbitrary values of $x$. We have done this for ortho concentrations corresponding to the experimental data displayed in Fig. 1 and 2. Figure 6 shows our results for $0.006 \leq x \leq 0.069$. All curves were calculated with $\mathrm{Im}E = 0.003$ $cm^{-1}$, which gives rise to a Lorentzian line shape function for pure $p$-$H_2$, as indicated by the broken curve along the baseline of the figure. The value of 0.003 $cm^{-1}$ was chosen to simulate the effects of finite instrumental resolution shown by the broken curve in Fig. 1. Figure 7 gives the corresponding results at higher concentrations of $o$-$H_2$, $x = 0.13$ and 0.19.

Taken together, Figs. 6 and 7 show very good agreement with the experimental results displayed in Figs. 1 and 2. Equally good agreement is obtained in the case of HD impurities, as shown by comparing Fig. 8 with Fig. 4. It is evident in both the experiment and the theory that the HD impurities have a smaller effect on the line shape than an equal concentration of $o$-$H_2$. This is explained by the fact that it is the ratio of bandwidth to intramolecular frequency difference that determines the influence of the impurities. In the case of $o$-$H_2$, one has $W/\Delta = 1.33$, whereas with HD, $W/\Delta = 0.015$.

As reported in detail in Ref. 5, both the ortho and the para peaks shift with increasing concentration of $o$-$H_2$. Using the formalism of the CPA, an approximate expression for the positions of the two peaks can be obtained from Eq. (4.5) by setting $E = V_c$ in the argument of the Green's function and solving the resulting quadratic

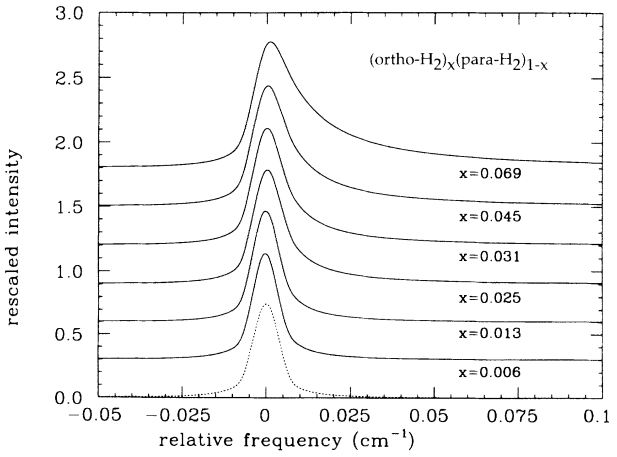


FIG. 6. CPA calculation of the optical line shape function of the $p$-$H_2$ vibron in mixed crystals of $(o\text{-}H_2)_x(p\text{-}H_2)_{1-x}$ for various $x$. The broken line indicates the limiting line shape for $x$ =0, corresponding to $\mathrm{Im}E = 0.003$ $cm^{-1}$. The curves were calculated with $\Delta = 3$ $cm^{-1}$ and $W = 4$ $cm^{-1}$. This figure is to be compared with Fig. 1.

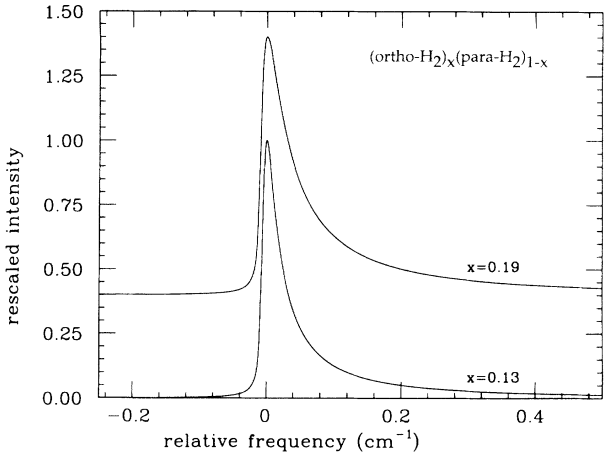


FIG. 7. CPA calculation of the optical line shape function of the $p$-$H_2$ vibron in mixed crystals of $(o\text{-}H_2)_x(p\text{-}H_2)_{1-x}$ for $x$= 0.13 and 0.19. Both curves are calculated with $\Delta$= 3 $cm^{-1}$, $W$= 4 $cm^{-1}$, and $\mathrm{Im}E = 0.003$ $cm^{-1}$. This figure is to be compared with Fig. 2.

equation for $V_c$. The two solutions are identified with the positions of the ortho and para peaks, $E_p$(ortho) and $E_p$(para). One finds

$$E_p(\text{ortho}) = \frac{1}{2}A - \frac{1}{2}\sqrt{(2\Delta - A)^2 + 8x\Delta A}, \tag{4.7}$$

and

$$E_p(\text{para}) = \frac{1}{2}A + \frac{1}{2}\sqrt{(2\Delta - A)^2 + 8x\Delta A}, \tag{4.8}$$

with $A = -1/G_o(0)$.

Figure 9 shows the CPA values for the shifts in the para and ortho peaks with increasing ortho concentration for $0 \leq x \leq 1$. The curves were calculated from Eqs. (4.7) and (4.8) with $\Delta = 3$ $cm^{-1}$ and $A = W/1.792 = 2.23$ $cm^{-1}$. Comparison with the data of Refs. 5 and 24 in-

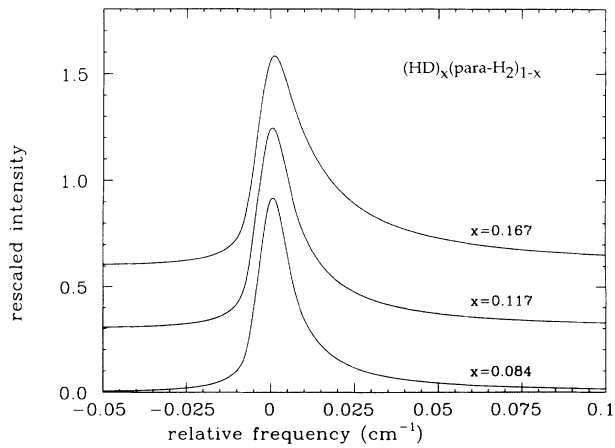


FIG. 8. CPA calculation of the optical line-shape function of the $p$-$H_2$ vibron in a mixed crystal of $(HD)_x(p\text{-}H_2)_{1-x}$ for $x$ = 0.084, 0.117, and 0.167. The curves are calculated with $\Delta = 264.5$ $cm^{-1}$, $W = 4$ $cm^{-1}$, and $\mathrm{Im}E = 0.003$ $cm^{-1}$. This figure is to be compared with Fig. 4.

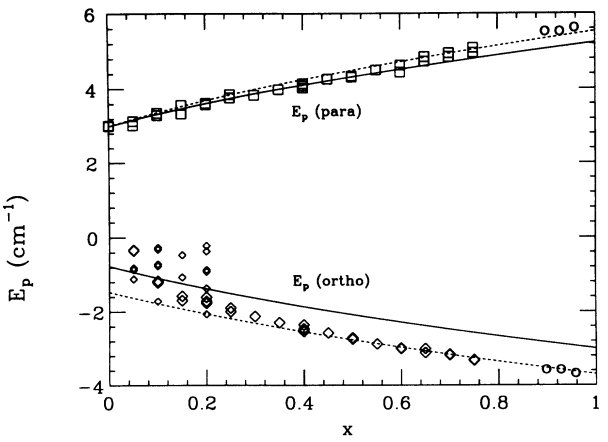


FIG. 9. CPA calculation of the positions of the para and the ortho peaks as a function of ortho concentration $x$ in $(o\text{-}H_2)_x(p\text{-}H_2)_{1-x}$. Upper curve: $E_p$(para); lower curve: $E_p$(ortho). The squares and diamonds are data from Table I of Ref. 5, with the smaller diamonds denoting less intense secondary peaks. The open circles denote the peak positions in the hcp phase ($T = 4.3$ K) reported in Ref. 24. The solid curves are calculated from Eqs. (4.7) and (4.8) with $A = 2.23$ cm$^{-1}$ and $\Delta = 3$ cm$^{-1}$. The dashed curves show the results obtained with $A = 2.53$ cm$^{-1}$ and $\Delta = 3.4$ cm$^{-1}$. They have been shifted downward by 0.4 cm$^{-1}$ so that $E_p$(para) matches the experimental value for the para peak in pure $p$-$H_2$. The zero of energy is at 4146.7 cm$^{-1}$, 3 cm$^{-1}$ below the peak in $p$-$H_2$.

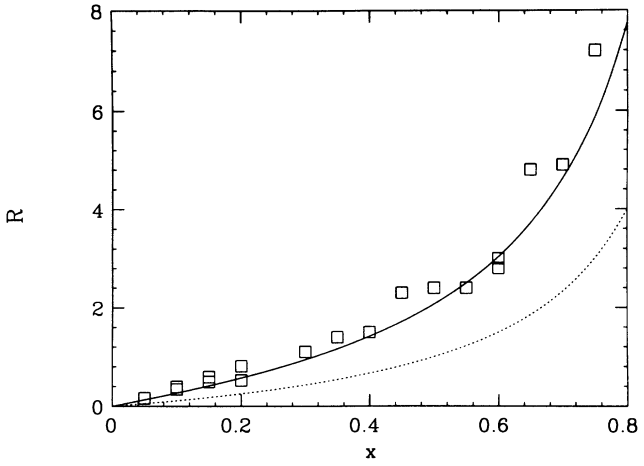


FIG. 10. CPA calculation of $R$, the ratio of the intensities of the ortho and para peaks, as a function of ortho concentration $x$. Open squares (□) denote the experimental results from Table III of Ref. 5. The solid curve is calculated from Eq. (4.10) with $A/\Delta = 0.743$. The dashed curve is the result for noninteracting molecules, $x/(1-x)$.

dicates there is good agreement between experiment and theory for the positions of the para peaks. In the case of the ortho peaks, there is only qualitative agreement, although the presence of less intense secondary peaks[5] arising from the electric quadrupole-quadrupole interaction between the ortho molecules makes the comparison somewhat imprecise at small $x$. However, it should be noted that better overall agreement for $x \geq 0.2$ can be obtained for slightly different values for $A$ and $\Delta$. The dashed curve in Fig. 9 displays the results for $A = 2.53$ cm$^{-1}$ ($W = 4.53$ cm$^{-1}$) and $\Delta = 3.4$ cm$^{-1}$, for which the ratio of $A$ to $\Delta$ is the same as for $A = 2.23$ cm$^{-1}$ and $\Delta = 3$ cm$^{-1}$. For $x \geq 0.2$, the disagreement between the experimental data and the solid curve can be traced to our approximation that the *intermolecular* interactions are the same for ortho and para molecules. The difference between $2\Delta$ and the spacing between the para peak in pure $p$-$H_2$ and ortho peak in pure $o$-$H_2$ is a measure of the difference between the ortho-ortho and para-para interactions, which arises from the electric quadrupole-quadrupole coupling.

The CPA also accounts for the relative intensities of the ortho and para peaks as a function of ortho concentration. In the spirit of the two-pole approximation of Eqs. (4.7) and (4.8), the optical line shape is given by the expression

$$f(E) = \frac{1}{\pi}\mathrm{Im}\left\{\frac{E + \int dV V P(V) - E_1 - E_2}{(E-E_1)(E-E_2)}\right\}. \quad (4.9)$$

Equation (4.9) is obtained from the corresponding expression for noninteracting molecules by rewriting $xE_1 + (1-x)E_2$ as $\int dV V P(V)$, where $P(V)$ is given by Eq. (4.4). This replacement ensures that the expression in curly brackets has the correct CPA behavior for *interacting* molecules in the large-$E$ limit, $|E| \gg \Delta, W$. In making this transcription, $E_1$ and $E_2$ are identified with $E_p$(ortho) and $E_p$(para), respectively. The resulting line shape is the sum of $\delta$ functions at $E_p$(ortho) and $E_p$(para) with weights $U$ and $1-U$ respectively, where $U$ is given by

$$U = \left[\frac{1}{2}\sqrt{\left(2-\frac{A}{\Delta}\right)^2 + 8x\frac{A}{\Delta}} - (1-2x) + \frac{1}{2}\frac{A}{\Delta}\right] \Bigg/ \sqrt{\left(2-\frac{A}{\Delta}\right)^2 + 8x\frac{A}{\Delta}}\,. \quad (4.10)$$

In Fig. 10 we display a plot of the ratio of the intensities of the ortho and para peaks, which we denote by $R = U/(1-U)$, along with the experimental results from Ref. 5 and the corresponding ratio in the absence of intermolecular interactions, $x/(1-x)$. The curve was calculated with $A/\Delta = 0.743$, which is the ratio associated with the $(A, \Delta)$ pairs generating the two sets of curves in Fig. 10. It is apparent from the figure that the CPA gives good agreement with the data over the whole range covered by the experiments.

## V. DISCUSSION

The observed broadening and the asymmetry of the $p$-$H_2$ vibrational line shapes in $(o\text{-}H_2)_x(p\text{-}H_2)_{1-x}$ mixed

crystals is not due to inhomogeneities, caused by the substitution of $p$-$H_2$ by $o$-$H_2$. While the $p$-$H_2$ and $o$-$H_2$ are two states of the same molecule, their different electron distribution may cause some different inhomogeneities. However, the symmetrical line shape of isolated $o$-$D_2$ stretching vibrations in the $(o\text{-}D_2)_{0.025}(p\text{-}H_2)_{0.907}(o\text{-}H_2)_{0.068}$ mixed crystal (see Sec. III C) clearly indicates that the asymmetry is not due to environmental inhomogeneities, but has an excitonic character.

The CPA scheme is well suited for the calculation of the line shape of these vibrational exciton states. Excellent agreement with the experimental spectra is attained. It also predicts the anomalous larger intensity of the $o$-$H_2$ stretching vibration compared to the $p$-$H_2$ transition and the shift of the vibrational frequencies of the $o$-$H_2$ and the $p$-$H_2$ transitions as a function of the $o$-$H_2$ concentration.

From the difference between doping with $o$-$H_2$ on the one hand and with HD or $o$-$D_2$ on the other hand, we see that the scattering is less efficient for impurities with a vibrational frequency which is much further off the frequency of the delocalized states. Hence, the small difference in vibrational frequency between the $o$-$H_2$ and the $p$-$H_2$ species makes the scattering "near-resonance."

For the highest $o$-$H_2$ concentration $x = 0.013$ and $x = 0.019$ the lower-frequency edge of the calculated line shape is much steeper than the experimental data (compare Figs. 1 and 2 with Figs. 6 and 7). This may have three causes: (i) The CPA model does not include any contributions to the line broadening due to the interactions with the phonons. This can be included by pragmatically convoluting[11] the line shape obtained by the CPA calculation with a Lorentzian. (ii) For those high $o$-$H_2$ concentrations, higher-order terms in the expansion of the Green's function $G_o(E)$ [Eq. (4.6)] should be included. (iii) The electrical quadrupole-quadrupole interaction among the ortho species, which was neglected in the calculations, may become important. Experimental results in crystals with higher concentrations of $o$-$H_2$ show indeed a more complex line shape and are not shown in this paper.

The FWHM of the $o$-$D_2$ transition in the $(o\text{-}D_2)_{0.025}(p\text{-}H_2)_{0.907}(o\text{-}H_2)_{0.068}$ mixed crystal is larger than the width of the $p$-$H_2$ vibron (see corresponding spectrum in Fig. 2), showing that the coupling between the vibrational states on different sites results in a "motional narrowing" of the vibration transition. This effect was already observed[4,25] for the vibrational states in $\alpha$-$N_2$ and $\beta$-$N_2$.

It should be noted that all the CPA results were obtained with a consistent set of parameters, i.e., values of $W$ and $\Delta$ that give results for the line shape which are in good agreement with experiment also account for the variation of the relative peak positions and ortho/para intensity ratio. Unlike earlier theories, which are limited to low impurity concentration,[13,26] the CPA is appropriate over the entire concentration range, $0 \leq x \leq 1$.

## ACKNOWLEDGMENTS

J.D.K. wants to acknowledge financial support from the National Fund for Scientific Research Belgium (NFWO). This work was made possible by further financial support from the Inter-University Institute for Nuclear Sciences (IIKW) and the Belgian national lottery. A.B. and D.L.H. (SRC) received support from the National Science Foundation under the Cooperative Agreement DMR-9212658.

* Also at Department of Physics, University of Wisconsin–Madison, Madison, Wisconsin 53706.

[1] P. Foggi and V. Schettino, Riv. Nuovo Cimento **15**, 1 (1992).
[2] E.L. Chronister and D.D. Dlott, J. Chem. Phys. **79**, 5286 (1983).
[3] J. De Kinder, A. Bouwen, E. Goovaerts, and D. Schoemaker, J. Chem. Phys. **95**, 2269 (1991); Phys. Rev. B **47**, 14 565 (1993).
[4] J. De Kinder, E. Goovaerts, A. Bouwen, and D. Schoemaker, Phys. Rev. B **42**, 5953 (1990).
[5] V. Soots, E.J. Allin, and H.L. Welsh, Can. J. Phys. **43**, 1985 (1965).
[6] J. Van Kranendonk and G. Karl, Rev. Mod. Phys. **40**, 531 (1968).
[7] C. Delalande and G.M. Gale, Chem. Phys. Lett. **50**, 339 (1977).
[8] I.I. Abram, R.M. Hochstrasser, J.E. Kohl, M.G. Semack, and D. White, Chem. Phys. Lett. **71**, 405 (1980).
[9] S. Velsko and R.M. Hochstrasser, J. Phys. Chem. **89**, 2240 (1985).
[10] P. Soven, Phys. Rev. **156**, 809 (1967).
[11] J. Hoshen and J. Jortner, J. Chem. Phys. **56**, 933 (1972); **56**, 5550 (1972).
[12] A.H. McKague Rosevear, G. Whiting, and E.J. Allin, Can. J. Phys. **47**, 3589 (1967).
[13] H.M. James and J. Van Kranendonk, Phys. Rev. **164**, 1159 (1967).
[14] See, for example, B.N.J. Persson and R. Ryberg, Phys. Rev. B **24**, 6954 (1981).
[15] C. Sierens, A. Bouwen, E. Goovaerts, M. De Mazière, and D. Schoemaker, Phys. Rev. B **37**, 4769 (1988).
[16] M. Leblans, A. Bouwen, C. Sierens, W. Joosen, E. Goovaerts, and D. Schoemaker, Phys. Rev. B **40**, 6674 (1989).
[17] I.F. Silvera, Rev. Mod. Phys. **52**, 393 (1980).
[18] I.I. Abram, R.M. Hochstrasser, J.E. Kohl, M.G. Semack, and D. White, J. Chem. Phys. **71**, 153 (1979).
[19] T. Momose, D.P. Wekily, and T. Oka, J. Mol. Spectrosc. **153**, 760 (1992); their spectra were recorded by the tone burst modulation technique, which yield second-order derivative spectra. We have converted their quoted numbers of second-order derivative spectra by a factor 6.1 to yield comparable quantities.
[20] M.-C. Chan, L.-W. Xu, C.M. Gabrys, and T. Oka, J. Chem. Phys. **95**, 9404 (1991); see remark in Ref. 19.

[21] A. Boukahil and D.L. Huber, J. Lumin. **45**, 13 (1990); Phys. Lett. A **159**, 353 (1991); J. Lumin. **48&49**, 255 (1991).
[22] G.K. Teal and G.E. Macwood, J. Chem. Phys. **3**, 760 (1935).
[23] A. Boukahil and D.L. Huber, Chem. Phys. **177**, 709 (1993).
[24] W.R.C. Prior and E.J. Allin, Can. J. Phys. **51**, 1935 (1973).
[25] J. De Kinder, A. Bouwen, and D. Schoemaker, Chem. Phys. Lett. **203**, 12 (1993).
[26] J. Van Kranendonk, *Solid Hydrogen* (Plenum, New York, 1983), Chap. 3.